LAWRENCE
LIVERMORE
NATIONAL
LABORATORY

UCRL-JRNL-211287

The Ring System of Uranus: Flat as a Pancake, Sprinkled with Dust

I. de Pater, S. G. Gibbard, H. B. Hammel

April 11, 2005

Icarus

The Ring System of Uranus: Flat as a Pancake, Sprinkled with Dust

Imke de Pater[1], Seran G. Gibbard[2], and Heidi B. Hammel[3]

[1] Astronomy Department, 601 Campbell Hall

University of California, Berkeley, CA 94720

imke@astron.berkeley.edu

[2]Lawrence Livermore National Laboratory

Livermore, CA 94550 USA

[3]Space Science Institute

4750 Walnut Street, Suite 205

Boulder, CO 80301

Submitted to Icarus 2004 Oct. 29.

Pages: 23 Tables: 3

Figures: 5 (Fig. 4 is in color)

Proposed running head: Uranus: Pancakes and Dust Rings

Editorial correspondence to:

Imke de Pater

Department of Astronomy

601 Campbell Hall, University of California

Berkeley, CA 94720

phone: 510-642-1947

FAX: 510-642-3411

E-mail: imke@astron.berkeley.edu

Abstract

We present a high quality image of the uranian ring system, obtained in July 2004 at 2.2 μmwith the adaptive optics camera NIRC2 on the Keck II telescope. Using these data, we report the first ground-based image of the ring 1986U2R, seen only once before by the Voyager spacecraft. We show that this ring extends inward to $\sim$ 7000 km above the Uranus cloud deck. Its VIF (total vertically integrated I/F) is $\approx$ 100 m. We further detected narrow sheets of dust in between the δ and ϵ rings, and in between rings 4 and α, with a VIF of 14 and 20 m, respectively.

Surprisingly, we find that the particles in Uranus' 9 main rings are distributed within a mono-layer, rather than the usually adopted poly-layer model. We come to this conclusion via a comparison of the VIF as derived from our 2003 data at a ring opening angle $B \approx 18^\circ$ (from Gibbard *et al.* 2004) with those derived in this paper at $B \approx 11^\circ$. We show that the VIF increases approximately as $1/\sin B$ at the ring ansae, but is independent of $\sin B$ in front of the disk. This combination of factors can only be explained if the particles in Uranus' rings are distributed in a mono-layer, a configuration which makes the uranian system unique amongst the giant planets.

keywords Planetary rings, Uranus, infrared observations.

1. Introduction

We have observed Uranus with the Adaptive Optics (AO) system on the 10-m W.M. Keck II telescope since the AO system was first commissioned at Keck, in 2000 (Wizinowich *et al.* 2000). At that time we recovered, for the first time from a ground-based telescope, the three groups of ringlets interior to the ϵ ring, and several cloud features both in Uranus' northern and southern hemispheres (Hammel *et al.* 2001; de Pater *et al.* 2002). In addition to these scientific results, we also noticed that the performance of AO observations of extended sources, such as Uranus, was not optimal: the Strehl ratio [the ratio of the peak intensity of the observed point spread function (PSF) to the theoretical maximum for the telescope aperture] was only a few %, and angular resolution roughly two times below the diffraction limit of the telescope (de Pater *et al.* 2002). These results were later used by the Keck AO team to optimize the system (van Dam *et al.* 2003, 2004), which lead to dramatic improvements in image quality (e.g., Gibbard *et al.* 2004; de Pater *et al.* 2004; Hammel *et al.* 2004a, b).

In order to track changes in Uranus' atmosphere and ring system while the viewing geometry of the planet, as seen from Earth and the Sun, is changing, we are monitoring the uranian system almost yearly. A summary of our data at K' band is shown in Fig. 1, with specifics on the observations in Table 1. Our first dataset was taken with the SCAM slit-viewing camera of the NIRSPEC spectrometer behind AO. SCAM has a 256 $\times$ 256 detector (McLean *et al.* 2000), covering a field of view of $4.5'' \times 4.5''$. Since Uranus + rings are $\sim 8''$ in extent, we observed the system in mosaic mode. In December 2001 the facility instrument near-infrared AO camera NIRC2 was partially commissioned, which in high resolution mode ($0.01''$ pixel size) gave a field of view of $10'' \times 10''$, large enough to image the uranian system in its entirety in one exposure. We were able to image the system just before Uranus set below the elevation limit of the telescope. In July/August of 2002 wea obtained much sharper images, as shown. In the following year, after AO optimalization,

our images showed much enhanced Strehl ratios and hence overall image quality. Satellite and ring particle reflectivities of all individual ringlets at J– (1.2 μm), H– (1.6 μm) and K'– (2.2 μm)–bands from our October 2003 observations were published by Gibbard *et al.* (2004), while Hammel *et al.* (2004a) presented a detailed analysis of the numerous cloud features seen in particular at J– and H–bands. In the present paper we present new results regarding Uranus' rings from our July 2004 data, with the first detection since the Voyager flyby in 1986 of the innermost known ring, or sheet of dust, 1986U2R. Hammel *et al.* (2004b) present results regarding atmospheric features detected during this period, in particular the first K' band detection of a cloud feature in Uranus' southern hemisphere, also shown in Fig. 1.

2. Observations

We observed Uranus and its ring/satellite system on UT 03, 04, 08, and 09 July 2004 with the Keck telescope on Mauna Kea, Hawaii. We used the AO system with NIRC2, a 1024 $\times$ 1024 Aladdin-3 InSb array. In this paper we present only K' band (1.948-2.299μ) observations of Uranus' rings. At this wavelength, sunlight is absorbed by methane and hydrogen gas in Uranus' atmosphere, greatly reducing scattered light from the planet; this permits ring material to be traced much closer to the planet. We used NIRC2 in high angular resolution mode, 9.94 $\pm$ 0.03 mas per pixel[1], which translates to 139.96 km/pixel. All images were processed using standard near-infrared data reduction techniques (flat-fielded, sky-subtracted, with bad pixels replaced by the median of surrounding pixels).

We obtained a typical spatial resolution of 0.04–0.05″ both on nearby stars and on unresolved satellites which were present on the Uranus images, and a Strehl ratio of $\sim$ 0.5. Since the satellites were observed simultaneously with Uranus, these observations

[1] We derived a pixel size of 0.00994 $\pm$ 0.00003″ from our data, using the known semimajor axes of the rings.

provide the most relevant AO parameters. Photometric calibrations were performed on star HD201941 (Elias *et al.* 1982). From these observations we derived a conversion factor of 3.1×10^{-4} with which to multiply the observed number of counts/sec/pixel to arrive at the I/F per pixel. I is the observed intensity and πF is the solar flux density as reflected from Uranus at K'.

Relevant ring parameters for the days that we observed are summarized in Table 2. On each half night we observed Uranus typically three times, where each observation usually consists of three sets of images, each integrated over 2 minutes. To obtain high signal-to-noise images of Uranus' rings, we carefully aligned all images and then combined all data. The total integration time on source is approximately 1.5 hrs. This process, of course, smears out any atmospheric features, such as those seen in Fig. 1, as well as satellites. Results of our final image are shown in Fig. 2. In panel a we show the image in its entirety, and panels b and c show enlarged views of the two ring ansae. These images clearly reveal the individual α, β and δ, γ, η rings, interior to the bright ϵ ring. Rings 4,5,6 cannot be resolved individually, but show up as an extended feature. Finally, interior to the 4,5,6 rings is a sheet of material which we believe is the ring 1986U2R, discovered by Voyager 2 in 1986 (Smith *et al.* 1986). Little is known about this ring; only one image of it was taken with Voyager, at a phase angle of 90°. The ring apparently has never even received a proper name; in this paper we refer to this ring as the ζ ring.

3. Image Analysis

3.1 Ring Models

In order to derive the I/F for the individual ringlets we need to either deconvolve the data, or build a model that, after convolution with the PSF, does match the observations. As in de Pater *et al.* (2002), we constructed models to fit the data by using both a 1D and 2D technique. In the 2D model, each of the 9 known rings (ϵ, δ, γ, η, β, α, 4, 5 and 6)

was represented as a single-pixel-wide ellipse at its appropriate distance from Uranus, with a single brightness (I/F value). The brightness of each pixel is scaled by the fraction of the pixel that would be occupied by the ring ellipse. In addition to the rings, we also added a (spherical) planet with constant brightness, equal to the average I/F of Uranus. We varied the brightness of each ring to find the best fit to the data (using the IDL AMOEBA routine, a downhill simplex method). Another free parameter was the azimuthal gradient in brightness in the ϵ ring. The other rings were assumed to be azimuthally invariant (see Gibbard *et al.* 2004). Finally, to represent the ζ ring, we added a uniform sheet of material interior to the 456 rings, with a variable width, location and I/F. This model was then convolved with the PSF, for which we used a nearby reference star (the PSF was an average of PSFs taken on the individual days). We minimized the errors between model and data by comparing north-south slices through each ansa, averaged over 10 pixels east-west. We did the analysis separately for the two ring ansae.

In the 1D analysis we simply used a north-south slice through the data, averaged over 4 pixels east-west, and fit this to a 1D model of the rings (i.e., like a slice through the 2D model). In this model we adopted a sheet of material interior to rings 456, consisting of several uniform rings rather than just one single-brightness sheet, to represent the ζ ring. We also removed scattered light from the planet in the 1D scans prior to modeling. The scattered light contribution was determined from east-west scans through the planet. We constructed a 1D PSF from the ring data themselves, so as to model the wings of the PSF as accurately as possible (de Pater *et al.* 2002): The ϵ ring is unresolved in our 1D scans, and the drop-off in intensity from the ϵ ring outwards mimicks the PSF. We used the scans through the ϵ ring away from Uranus both on the north and south sides. The PSF appeared to be symmetric, and we averaged the two traces after flipping them.

In Figs. 3a and 3b we show 1D scans through the rings south and north, averaged over 4 pixels east-west, with superposed our best 1D model fit. In Figs. 3c and 3d we

show the same results for our 2D model fits, where the scans were averaged over 10 pixels east-west (this explains the difference in peak intensities between the 1D and 2D scans). As mentioned above, the rings in the 2D models were represented by single-pixel wide ellipses for the 9 known rings, while the inner ζ ring was modeled by an extended sheet. As shown, both 1D and 2D models fit the peak values in each ring quite well, but fail to match the minima between the α and 456 rings, and between the δ and ϵ rings. In the latter region the 1D models provide a slightly better fit than the 2D models, presumably caused by a better representation of the PSF (wings); however, the fit is far from perfect. We note that this problem did not occur in the 2003 data, which were modeled using the same 2D model technique (Gibbard *et al.* 2004), nor in the 2000 data (de Pater *et al.* 2002; but the angular resolution and image quality was lower in these data). Hence, we believe that the mismatch between model and data cannot be attributed to inaccuracies in the PSF. We suggest, instead, that the regions in between the rings do contain material, most likely dust at low optical depth. The reason we 'see' this dust now, but not in previous years, is the change in viewing geometry. The relatively low ring opening angle in 2004 ($\sim 11^\circ$) allows for a longer line-of-sight pathlength through the rings compared to previous years. For example, the pathlength is a factor of 1.63 longer in 2004 than in 2003.

To more accurately reproduce the ring profiles, we modified our 1D models by adding dust sheets between rings α and 4, and in between the ϵ and δ rings, as indicated by the cyan-colored dotted lines in Fig. 4. This model, convolved with the PSF, is shown by the red dashed line, which is almost indistinguishable from the data (solid black line). In the bottom panel we show the difference between the model and data, multiplied by a factor of 5. On this figure we also show our best characterization of the ζ ring: a uniform sheet of material with a width of $\sim$ 3500 km at an I/F of 1.8×10^{-5}, which is centered 39,600 km from Uranus. Our 2D model fits were compatible with these results; they yield a $\sim$ 2000 km wide sheet of material at $I/F \approx 4 \times 10^{-5}$, at 39,340 km from Uranus. Our 1D fits also required a step-like (or perhaps gradual) decrease in intensity closer to Uranus, as indicated

in the figures (cyan dotted lines); the data could not be fit without dust being present down to $\sim$ 7000 km above Uranus' cloud deck (note that scattered Uranus light was subtracted, so did not influence these results). Although the absolute I/F of the ζ ring on the north side was slightly smaller than on the south side (1.6×10^{-5} vs 2.0×10^{-5}), the decrease in intensity closer to Uranus relative to the main sheet of dust is the same.

3.2 I/F Results

In order to obtain an single representative I/F for the ring system, we average the I/F for the north and south ansae. Since the width (and hence brightness) of the Uranus ϵ ring, as well as most of the other rings, varies approximately sinusoidally with azimuth (French *et al.* 1986), this simple average of two values 180 degrees apart in azimuth gives the average ring brightness. To facilitate comparison with other data, we express the I/F as an integrated quantity, i.e., integrated vertically across the rings, in the plane of the sky, as shown schematically in Fig. 5:

$$VIF = \int \frac{I}{F}(z)dz. \tag{1}$$

VIF is thus the equivalent extent of a ring (in m) if the ring had a reflectivity $I/F = 1$ (i.e., a perfect Lambertian reflector) (e.g., Scharringhausen *et al.* 2001; de Pater *et al.* 2002 – the latter authors referred to this quantity as EW, or equivalent I/F width) We calculate VIF_{ansa} from our modeled I/F values by multiplying each ring's I/F (a dimensionless quantity) by the pixel size in meters. Column 2 in Table 3 shows the results for our 2004 data. The uncertainty is a conservative estimate based upon our fits; clearly, the relevant uncertainty is dominated by photometric errors, which, based upon night-to-night observations, we believe to be less than 5%. We note that, for the ϵ ring, we can perform the integration in eq. (1) directly on the north-south scans. After multiplication by the pixel size in m, this integration yields the same VIF value as listed in Table 3.

Column 3 in Table 3 shows the ratios in VIF between the south and north sides of the rings. The ratio of ring brightness at periapse to the brightness at apoapse is designated q. The values given in the table are not the same as q, since the ring apo– and peri-apses are not at the ring ansae. However, for rings with a sinudoidal variation such as the ϵ ring, the north/south ratio, referred to as q', yields a lower limit to q. We find $q' = 2.5$ for the ϵ ring, somewhat less than the apo– to peri-apse ratio $q = 3.5 \pm 0.1$, as measured directly on the image at apo– and peri-apse. All other rings, with the exception of the η ring, show azimuthal brightness variations at the 10 – 20% level, up to $\sim$ 30% for ring 456. Such q' values agree with the numbers presented by Gibbard *et al.* (2004). Rings 456 are also clearly eccentric: the rings are $\sim$ 70 km closer to Uranus in the north (near pericenter; lower I/F) than in the south, in agreement with the asymmetry expected for rings with an eccentricity $\sim$ 0.001 (Murray and Dermott, 1999).

Column 4 shows the VIF results from Gibbard *et al.* (2004) for our October 2003 data, averaged over the J–, H–, and K'–band data, where the uncertainty is derived from the spread in the VIF values. We opted to average the I/F values at all bands, since the ring particle reflectivities do not show a wavelength dependence. In column 5 we show the ratio of the 2004/2003 data.

4. Discussion

4.1 Ring Models: Background

Rings are usually depicted as a collection of particles with a broad size distribution, such that the number of particles $N(R) \propto R^{-a}$, with R the radius of the particle and $a \approx 3$ for a collisionally evolved population of particles. Saturn's rings are usually adopted as the 'archetype' ring system. Poynting Robertson drag may lead to a loss of the smallest (μm-sized) particles (e.g., Broadfoot *et al.* 1986). The largest ones, which dominate the mass, should evolve into a 'dynamical mono-layer', or a ring with a thickness typically up to $\sim$

10 ring particle diameters across (Cuzzi *et al.* 1979), with the smaller sized fragments and dust in a many-particle thick 'poly-layer' or 'multi-layer'. Lane *et al.* (1986) showed from observations with the Voyager photopolarimeter during a stellar occultation event that the thickness of the edge of Uranus' ϵ ring was less than 150 m, the ring particles less than 30 m across, and that there was little or no dust in the ϵ ring. There appears to be no wavelength dependence in the optical depth of Uranus' rings (except in the λ ring), as measured over a large range of wavelengths (0.11 μm up to 13 cm), indicative of an absence of particles less than a few cm across. This, together with detailed analyses of Voyager occultation profiles, constrains the particle sizes in Uranus' rings to a range between $\sim$ 10 cm and 10 m, with an effective size of a few m (e.g., French *et al.* 1991; Esposito *et al.* 1991).

To determine whether the uranian ring system is similar to Saturn's, e.g., a multi-layered ring, or whether the particles are distributed in a single layer, Elliot *et al.* (1984) and French *et al.* (1986) analyzed occultation profiles of Uranus' rings, and introduced the concept of equivalent width (E) and equivalent depth (A):

$$E = W(1 - e^{-\tau})\sin B \tag{2}$$

$$A = W\tau\sin B, \tag{3}$$

with W the width of the ring, τ the optical depth, and B the ring opening angle. They show that E does not vary with B for a mono-layer of particles, while A does not vary with B for a poly-layer. From a detailed analysis of E and A as a function of W and the true anomaly, French *et al.* (1986) concluded that the rings, according to their occultation profiles, were most likely many particles thick.

Karkoschka (2001a) used this concept to develop a model for the rings based upon Irvine's (1966) scattering model. His model accounts for reduced shadowing between ring

particles when the planet is near opposition, as expected for a many-particle thick ring. Karkoschka adopted a filling factor of 0.06, i.e., only 6% of the rings are filled with ring particles. Based upon this model, he provides the visible area of ring particles, that is, the total cross section of the rings minus any gaps, holes or shadows, as a function of subsolar latitude and phase angle. This visible area, multiplied by the ring particle reflectivity, results in the ring's I/F, a value that can be directly observed. Gibbard *et al.* (2004) used this model to derive the ring particle reflectivity from their observed I/Fs in each ringlet. They derived a typical value of ~ 0.044 at a phase angle of $\sim 2°$, in excellent agreement with the numbers found by Karkoschka (2001b; 0.3–1 μm) and de Pater *et al.* (2002; 1.6–2.2 μm) at similar phase angles, and hence confirmed a neutral color for the rings.

In addition to changes in the ring's visible area, Karkoschka (2001a) also used his model to predict the change in the ϵ ring's azimuthal brightness variation as a function of subsolar latitude and phase angle. He predicts that the ratio q of the ϵ ring's brightness at apoapse to periapse will increase from about 2 to 5 when we approach ring plane crossing in 2007. Table 1 shows q for the data displayed in Fig. 1. The gradual increase in q from 2.7 in 2000 to 3.5 in 2004 agrees with Karkoschka's (2001a) predictions.

Although Karkoschka's (2001a) model is the most sophisticated we have to date, it still is a model with a number of underlying assumptions. It is a single-scattering multi-layered model, filled with spherical particles of a constant size. The model includes shadowing, which enhances the opposition effect. Via comparison with HST and Voyager data, Karkoschka determined a best value of 0.06 for the average filling factor (in the ϵ ring the filling factor ranges from 0.04 at apoapse to 0.18 at perapse). He shows, however, that this filling factor needs to be increased by a factor of ~ 3 if a particle size distribution rather than a single particle size is used, and hence 0.06 presents a lower limit to the filling factor. On the other hand, radio occultation data suggest filling factors of the order of 0.01 or less, which are inconsistent with Karkoschka's model (Tyler *et al.* 1986; Gresh *et al.* 1989).

Both q and the ring's visible area in Karkoschka's model change most rapidly at subsolar latitudes $\lesssim 15°$. Hence, observations of the ring's I/F while the rings are closing up form an excellent test of Karkoschka's model, and can be used to improve the model if need be. In addition, through such observations we believe we can address the issue of a possible mono– versus poly-layer configuration.

4.2 Particle Distribution in the Rings: Mono-layer or Poly-layer?

Column 5 in Table 3 lists the ratio in VIF_{ansa} between our 2004 and 2003 data. This ratio, for most rings, is very close to the ratio in $\mu = \sin B$, with B the ring opening angle: $\mu_{2003}/\mu_{2004} = 1.63$. Only for rings 456 is the ratio larger than 1.63. This high observed value might be caused by an underestimate of the rings' I/F in 2003, because these rings are very faint and very close to Uranus. If the discrepancy is real, though, it suggests the presence of low optical depth dust embedded within and/or in between these faint rings. The ratio for the γ ring may be lower than for the other rings; however, given the error-bar, we do not find this statistically significant.

As shown below, it would also be useful to determine VIF_{front} (Fig. 5). Unfortunately, because of the foreshortening effect, it is much more difficult to separate the individual rings in front of the planet than on the ansae. The ϵ ring, though, is clearly recognized in east-west scans. With the known azimuthal asymmetry of this ring, however, a single measurement of VIF_{front} is not very useful without its complement 180° away (i.e., behind the planet). Fortuitously, though, the pericenters of the ϵ ring differ by only 15° between our 2003 (125°) and 2004 (140°) observing sessions, and hence a comparison of VIF_{front} between both years is a meaningful quantity. We constructed east-west (relative to the planet) scans on both the 2003 and 2004 images by averaging over 40 rows of pixels, centered on the planet's center. We determined VIF_{front} directly from the scans (i.e., using eq. (1), rather than the detailed modeling process used to determine VIF_{ansa} in Table 3). We find that VIF_{front} in October 2003 equals 440 ± 40 m for the ϵ ring. In 2004 we find $VIF_{front} = 433 \pm 25$ m, resulting in a

ratio $VIF_{front}(2004)/VIF_{front}(2003) = 0.98 \pm 0.1$, i.e., independent of viewing angle. We note that the ϵ ring is unresolved; hence, in both years we integrated over the same number of pixels (9 pixels in z, Fig. 5). We also determined VIF_{front} integrated over all rings. After subtraction of the ϵ ring, we find $VIF_{front}(2004)/VIF_{front}(2003) = 0.8 \pm 0.2$ for all other rings combined. Since the overall shape of the ring profile is dominated by the PSF, we again integrated over the same number of pixels (24 in z) both years. Given the large uncertainties in our measurements, we conclude that this ratio is not significantly different from unity.

To summarize our findings: VIF_{ansa} varies in proportion with $1/\mu$ for all 9 rings, and VIF_{front} is independent of μ for the ϵ ring, and for all other 8 rings combined. We conclude from the latter observation that VIF_{front} is most likely independent of μ for all 9 rings. In order to understand what this observation tells us about the rings, we investigate below what μ dependence one might expect for different types of rings.

We distinguish between multi-layered rings and a mono-layer. For a poly-layer, where radiative transfer through the rings becomes important, we consider the two extreme situations of an optically thin and an optically thick ring. Each ring is less than 1 pixel wide (unresolved). We further assume that the viewing geometry of Uranus is the same as seen from Earth and the Sun (this is a reasonable asumption, since the phase angle is usually $\lesssim 2^\circ$), so, for simplicity, we deal with only one μ factor.

- *Poly-layer: Optically thick ring,* $\tau >> 1$*:*

  $VIF_{front} \propto \mu$, since the visible area (within a pixel) varies with μ.

  VIF_{ansa} is independent of μ, since the visible area within a pixel is constant.

- *Poly-layer: Optically thin ring,* $\tau << 1$*:*

VIF_{front} is independent of μ, since although the visible area is decreasing with μ, the total amount of material along the line-of-sight is increasing by $1/\mu$.

$VIF_{ansa} \propto 1/\mu$, since the line-of-sight through a pixel traverses through $1/\mu$ times more material.

- *Mono-layer:*

VIF_{front} is independent of μ, until ring particles block each other.

$VIF_{ansa} \propto 1/\mu$, until ring particles block each other.

If Uranus' rings are poly-layers, our data indicate that the rings must be optically thin, i.e., like a thin dust sheet, such as Jupiter's rings (e.g., Showalter *et al.* 1987; de Pater *et al.* 1999; Ockert-Bell *et al.* 1999) or Saturn's E ring (e.g., Larson *et al.* 1982; Nicholson *et al.* 1996; de Pater *et al.* 1996, 2004). As outlined above, this disagrees with everything we know about Uranus' ring system. The normal optical depth of the 9 main rings is typically between a few tenths up to $\sim$ 2 (Elliot *et al.* 1984), and ring occultation data show an absence of small-sized dust within the narrow main rings. Hence, the increase in VIF_{ansa} with $1/\mu$ between 2003 and 2004 cannot be explained via the line-of-sight effect of optically thin rings. This leaves us only one alternative, namely that the ring particles are distributed in a mono-layer. As discussed in the beginning of Section 4.1, such a distribution is conceivable if Uranus rings contain a more uniform big-boulder-like particle distribution.

4.3 Dust in Uranus' Ring System

4.3.1 ζ Ring (1986U2R)

Our observations clearly reveal a broad diffuse ring interior to rings 456, which we refer to as the ζ ring. This ring is located between 37,850 and 41,350 km, with a VIF of 63 $\pm$ 5 m. We believe this is the same ring as 1986U2R, discovered by Voyager in 1986, between

$\sim$ 37,000 and 39,500 km. Voyager obtained only one image of this ring at a phase angle of 90°. In addition to identifying the main sheet of material in this ring, we also show the presence of an extension at lower brightness ($VIF = 39 \pm 5$ m), that extends inward to 32,600 km from Uranus, about 7000 km above the planet's cloud deck. The brightness of this extension gradually decreases with decreasing distance from Uranus, as indicated on Fig. 4.

4.3.2 Dust in between the Main Rings

In addition to the recovery of the ζ, or 1986U2R, ring, we also detected dust in between rings ϵ and δ, and in between rings α and 4, at a total VIF of $\sim$ 14 and 20 m, respectively. Voyager 2 discovered large sheets of dust in between the classical rings in forward scattered light. A radial brightness scan through the high-phase Voyager image is shown by Esposito *et al.* (1991). This scan clearly shows the presence of dust between the δ ring at 48,300 km and the λ ring (including λ) at 50,000 km. We modeled this dust as a $\sim$ 175 km wide ring of uniform brightness, centered near 49,500 km. The ring is slightly ($\sim$ 250 km) closer to Uranus in the north than in the south. The observed profile cannot be matched with a uniform ring that exceeds $\sim$ 200 km.

There is also dust in between rings 4 and α in the Voyager 2 image, more or less concentrated in a strip between 42,700 and 43,700 km. Our data reveal a dust at 43,800 km, with a width of 350 km. We did not incorporate the Voyager low-brightness dust at 46,400 – 46,900 km, between the β and η rings; we note, however, that inclusion of dust at this location might improve our fit. Finally, just interior to ring 6 there is a concentration of dust at 41,000 – 41,350 km. As mentioned above, in our 1D model fits the ζ ring has to extend continuously outward to 41,350 km. We cannot fit the data with a narrow ring between 41,000 and 41,350 km, a gap, and a ζ ring inwards from 40,400 km.

5. Conclusions

In this paper we have presented the highest signal-to-noise K' band image of the uranian ring system obtained to date. The data were taken in July 2004 with the adaptive optics camera NIRC2 on the Keck II telescope. We have identified a sheet of material interior to the rings 456, referred to as the ζ ring, which we identified with the Voyager ring 1986U2R. In addition to a more or less uniform sheet of dust between 37,850 and 41,350 km with a vertically integrated $VIF = 63 \pm 5$ m, we find that the ring extends inward to $\sim$ 7000 km above the cloud tops at a much lower brightness, with $VIF \approx 40$ m. In addition to the ζ ring, we also detected narrow (few 100 km wide) sheets of dust between the δ and ϵ rings, and between rings 4 and α, at a VIF of $\sim$ 14 and 20 m for each ring, respectively.

A comparison of the VIF for each ring as derived from our 2003 data (at $B \approx 18°$; Gibbard *et al.* 2004) with those derived in this paper ($B \approx 11°$) shows an increase at the ansae that is approximately proportional to the ratio in $1/\mu$ ($\mu = \sin B$). In contrast, VIF in front of the rings is independent of μ. The combination of these findings can only be explained if the particles in Uranus' rings are distributed in a mono-layer, rather than in a multi– or poly-layer, as usually assumed. Such a mono-layer of particles has not been seen in any other ring system. Voyager observations showed that the main rings consist of large ($\gtrsim$ m-sized) boulders rather than the conventional particle size distribution with a preponderance of dust. Our data are the first to show that these particles are distributed in a mono-layer of material.

We plan to continue our observations of Uranus while the ring opening angle decreases. With increased values of $1/\mu$, our sensitivity to dust in the uranian system will increase, and we expect to refine our findings on both the ζ ring and on dust embedded within the uranian ring system. Continued observations of the VIF of the individual rings with increasing $1/\mu$ would help to refine ring models, such as Karkoschka's (2001a) poly-layered model. Within the mono-layer hypothesis, we expect the VIF at the ansae to increase with

$1/\mu$ until particles start to shadow each other. Such data will thus help constrain particle sizes and filling factors in the rings.

Acknowledgements

We thank Phil Nicholson for insightful discussions regarding ring geometries (and factors of μ). The data presented in this paper were obtained at the W. M. Keck Observatory, which is operated as a scientific partnership among the California Institute of Technology, the University of California and the National Aeronautics and Space Administration. The Observatory was made possible by the generous financial support of the W. M. Keck Foundation. This particular study was partially supported by the National Science Foundation and Technology Center for Adaptive Optics, managed by the University of California at Santa Cruz under cooperative agreement No. AST-9876783. It was further partially supported under the auspices of the U.S. Department of Energy, National Nuclear Security Administration by the University of California, Lawrence Livermore National Laboratory under contract No. W-7405-Eng-48, and by NASA grants NAG5-11961 and NAG5-10451.

The authors wish to recognize and acknowledge the very significant cultural role and reverence that the summit of Mauna Kea has always had within the indigenous Hawaiian community. We are most fortunate to have the opportunity to conduct observations of Uranus from this Hawaiian volcano.

References

Broadfoot, A.L., + 18 co-authors, 1986. Ultraviolet spectrometer observations of Uranus. Science 233, 74-79.

Cuzzi,J.N., Burns,J.A., Durisen,R.H., Hamill,P.M., 1979. The vertical structure and thickness of Saturn's rings. Nature 281, 202-204.

de Pater, I., Gibbard, S.G., Macintosh, B., Roe, H.G., Gavel, D., and Max, C.E., 2002. Keck Adaptive Optics Images of Uranus and its Rings. Icarus 160, 359-374.

de Pater, I., Gibbard, S.G., Chiang, E., Hammel, H.B., Macintosh, B., Marchis, F., Martin, S.C., Roe, H.G., and Showalter, M., 2004. The dynamic neptunian ring arcs: Gradual disappearance of Liberté and a resonant jump of Courage. Icarus, in press.

de Pater, I., Martin, S., and Showalter, M.R., 2004. Keck 2 μm Observations of Saturn's E and G Rings during Earth's ring plane crossing in August 1995. Icarus, in press.

de Pater, I., Showalter, M.R., Lissauer, J.J., Graham, J.R., 1996, Keck infrared observations of Saturn's E and G rings during Earth's 1995 ring plane crossing. Icarus Note 121, 195-198.

de Pater, I., Showalter, M.R., Burns, J.A., Nicholson, P.D., Liu, M.C., Hamilton, D.P., Graham, J.R., 1999. Keck infrared observations of Jupiter's ring system near Earth's 1997 ring plane crossing. Icarus 138, 214-223.

Elias, J.H., Frogel, J.A., Matthews, K., and Neugebauer, G., 1982. Infrared standard stars. Astron. J. 87, 1029-1034.

Elliot, J.L., French, R.G., Meech, K.J., and Elias, J.H., 1984. Structure of the Uranian rings. I. Square-well model and particle-size constraints. Astrophys. J. 89, 1587-1603.

Esposito, L.W., Brahic, A., Burns, J.A., and Marouf, E.A., 1991. Particle properties and processes in Uranus' rings. In Uranus (J.T. Bergstrahl, E.D. Miner, and M.S. Matthews, Eds.) Univ. of Arizona Press, Tucson, pp. 410-465.

French, R.G., Elliot, J.L., and Levine, S.E., 1986. Structure of the Uranian rings. II. Ring orbits and widths. Icarus 67, 134-163.

French, R.G., Nicholson, P.D., Porco, C.C., and Marouf, E.A., 1991. Dynamics and structure of the Uranian rings. In Uranus, Eds. J.T. Bergstrahl, E.D. Miner, M.S. Matthews. Univ. of Arizona Press, Tucson, AZ. pp. 327-409.

Gibbard, S.G., de Pater, I., and Hammel, H.B., 2004. Near-infrared Adaptive Optics Imaging of the Satellites and Individual Rings of Uranus from the W.M. Keck Observatory. Icarus, in press.

Gresh, D.L., Marouf, E.A., Tyler, G.L., Rosen, P.A., and Simpson, R.A., 1989. Voyager radio occultation by Uranus' rings. Icarus 78, 131-168.

Hammel, H.B., Rages, K., Lockwood, G.W., Karkoschka, E., and de Pater, I., 2001. New measurements of the winds of Uranus. Icarus 153, 229-235.

Hammel, H.B., de Pater, I., Gibbard, S.G., Lockwood, G.W., and Rages, K., 2004a. Uranus in 2003: Zonal winds, banded structure, and discrete features. Icarus, submitted. June 2004.

Hammel, H.B., de Pater, I., Gibbard, S.G., Lockwood, G.W., and Rages, K., 2004b. New cloud activity on Uranus in 2004: First detection of a southern feature at 2.2 microns. Icarus Note, submitted July 2004

Irvine, W.M., 1966. The shadowing effect in diffuse reflection. J. Geophys. Res. 71, 2931-2937.

Karkoschka, E., 2001a. Photometric modeling of the epsilon ring of Uranus and its spacing of particles. Icarus 151, 78-83.

Karkoschka, E., 2001b. Comprehensive photometry of the rings and 16 satellites of Uranus with the Hubble Space Telescope. Icarus 151, 51-68.

Lane, A.L., + 10 co-authors, 1986. Photometry from Voyager 2: Initial results from the Uranian atmosphere, satellites and rings. Science 233, 65-70.

Larson, S. M., Fountain, J.W., Smith, B.A., Reitsema, H.J., 1982. Observations of the Saturn E Ring and a new satellite. Icarus 47, 288-290.

McLean, I., Graham, J.R., Becklin, E.E., Figer, D.F., Larkin, J.E., Levenson, N.A., Teplitz, H.I., 2000. Performance and results with the NIRSPEC echelle spectrograph on the Keck II telescope. Proc. SPIE 4008, p. 1048-1055, Optical and IR Telescope Instrumentation and Detectors, Masanori Iye; Alan F. Moorwood; Eds.

Murray, C.D., and Dermott, S.F., 1999. Solar System Dynamics, Cambridge Univ. Press.

Nicholson, P.D., Showalter, M.R., Dones, L., French, R.G., Larson, S.M., Lissauer, J.J., McGhee, C.A., Seitzer, P., Sicardy, B., Danielson, G.E., 1996. Observations of Saturn's ring-plane crossing in August and November 1995. Science 272, 453-616.

Ockert-Bell, M.E., Burns, J.A., Dauber, I.J., Thomas, P.C., Veverka, J., Belton, M.J.S., and Klaasen, K.P., 1999. The structure of the jovian ring system as revealed by the Galileo imaging experiment. Icarus 138, 188-213.

Scharringhausen, B. R., Lim, L., Nicholson, P.D., Matthews, K., McGregor, P.J., 2001. Ground-Based Observations of the 10 August 1995 Saturn Ring-Plane Crossing. Icarus 154, 287-295.

Showalter, M.R., Burns, J.A., Cuzzi, J.N., Pollack, J.B., 1987, Jupiter's ring system: new results on structure and particle properties, Icarus 69, 458- 498.

Smith, B.A., + 39 co-authors, 1986, Voyager 2 in the Uranian system: Imaging science results, Science 233, 43-64.

Tyler, G.L., Sweetnam, D.N., Anderson, J.D., Campbell, J.K., Eshelman, V.R., Hinson, D.P., Levy, G.S., Lindal, G.F., Marouf, E.A., Simpson, R.A., 1986, Voyager 2 Radio Science observations of the Uranian system: atmosphere, rings, and satellites, Science 233, 79-84.

van Dam, M.A., and Macintosh, B.A., 2003. Characterization of adaptive optics at Keck Observatory, SPIE 5169, 1-10.

van Dam, M.A., Le Mignant D., and Macintosh, B.A., 2004. Performance of the Keck Observatory adaptive optics system. Applied Optics 43, 5458-5467.

Wizinowich, P.L., + 17 authors, 2000. First Light Adaptive Optics Images from the Keck II Telescope: A New Era of High Angular Resolution Imagery. PASP 112, Issue 769, pp. 315-319.

Figure Captions

Fig. 1. Uranus and its rings observed with Adaptive Optics on the Keck II telescope over the years 2000 – 2004. Specifics on the data are given in Table 1. The images from 2001 – 2004 are taken at a wavelength of 2.2 μm; the image in 2000 was taken in NIRSPEC's N6 filter, covering most of the H and K bands combined. Because of the H-band contribution, Uranus looks very different in this image compared to the later ones.

Fig. 2. Keck AO image of Uranus at 2.2 μm, after combining all data. The entire image is shown in panel a; panels b and c show the north and south ansae, respectively.

Fig. 3. North-south scans through the rings, with superposed models as detailed in the text. Panels a and b show scans averaged over 4 pixels east-west; panels c and d show scans averaged over 10 pixels east-west. The models are 1D models in the top panels, and 2D models at the bottom.

Fig. 4. North-south scans through the rings (averaged over 4 pixels east-west), with superposed the best-fit 1D models (dashed red line). The cyan colored dotted lines show the various dust sheets in our model, multiplied by a factor of 10 in I/F for clarity. The dotted blue lines show the I/F for the individual rings, divided by a factor of 5 for clarity. The bottom trace shows the the difference between the model and data, multiplied by a factor of 5. Both positive and negative deviations from zero are shown.

Fig. 5. Geometry of Uranus, and the direction over which VIF_{ansa} and VIF_{front} are integrated. (Adapted from the ringnode: http://pds-rings.arc.nasa.gov/)

Table 1. Observations in Figure 1

UT Time yr/month/day	Camera	Wavelength μm	Δ AU	r_o AU	Ang.Diam. $''$	B $^\circ$	Sun lat. $^\circ$	Phase angle $^\circ$	q	Reference
2000-06-18	SCAM	N6 (1.56-2.31)	19.32	19.40	3.65	26.7	29.0	2.34	2.7± 0.2	de Pater *et al* 2002
2001-12-18	NIRC2	K' (1.95-2.30)	20.52	19.99	3.43	25.4	23.1	2.32	2.5 ± 0.2	
2002-08-02	NIRC2	K'(1.95-2.30)	19.04	20.00	3.70	19.8	20.7	0.9	2.7 ± 0.2	
2003-10-05	NIRC2	K'(1.95-2.30)	19.28	20.03	3.66	18.1	16.2	1.93	3.2 ± 0.16	Gibbard *et al* 2004
2004-07-04	NIRC2	K'(1.95-2.30)	19.44	20.05	3.63	10.9	13.2	2.35	3.5 ± 0.1	Hammel *et al* 2005 + this paper

Δ = geocentric distance; r_o = heliocentric distance; Ang.Diam.= angular diameter; B = ring opening angle; Sun Lat. = Sun's latitude. q = ratio apoapse/periapse for ϵ ring.

Table 2. Ring Parameters on UT July 3/4 and 8/9, 2004

Ring	Distance (10^3 km)	Pericenter 03-04 July	Pericenter 08-09 July
Six	41.8	73-76°	87-90°
Five	42.2	182-185 °	195-198°
Four	42.6	128-130°	140-143°
Alpha	44.7	179-181°	190-192°
Beta	45.7	325-327°	335-337°
Eta	47.2	0°	0°
Gamma	47.6	318-320°	327-329°
Delta	48.3	0°	0°
Epsilon	51.1	135-137°	142-143°
Δ		2.908 $\times 10^3$ km	2.898 $\times 10^3$ km
r_0		2.999 $\times 10^3$ km	2.999 $\times 10^3$ km
Ring opening angle		10.9°	11.0°
Sub-solar latitude		13.25°	13.21°
Phase angle		2.35°	2.21°

Table 3. I/F **of the rings**

Ring	VIF_{ansa} 2004[1]	q'^2 q'^2	VIF_{ansa} 2003[3]	VIF_{ansa} 2004/2003[4]	Comments Comments
ϵ	1918± 15	2.52	1151± 40	1.67 ± 0.14	
δ	259 ± 7	1.17	165 ± 37	1.57 ± 0.37	
γ	113 ± 3	1.18	85 ± 24	1.33 ± 0.39	
η	266 ± 7	1.02	150 ± 37	1.77 ± 0.40	
β	269 ± 7	0.90	162 ± 23	1.66 ± 0.26	
α	267 ± 7	0.91	157 ± 18	1.70 ± 0.22	
$\delta+\gamma+\eta$	640 ± 16	1.10	400 ± 60	1.60 ± 0.26	
$\beta+\alpha$	536 ± 13	0.90	319 ± 30	1.68 ± 0.20	
4+5+6	259 ± 7	1.33	121 ± 16	2.14 ± 0.33	
ζ	63 ± 5				main sheet; 3500 km wide
ζ_c	39 ± 5				$\sim$ 5000 km sheet interior to ζ
$\text{dust}_{\alpha-4}$	20 ± 3				385 km wide
$\text{dust}_{\epsilon-\delta}$	14 ± 2				175 km wide

1 $VIF(ansa$ is expressed in m, assuming 139.96 km/pixel; the uncertainties are based upon the 1D fits.

2 The ratios in VIF_{ansa} between the south and north sides of the rings (i.e. not apo/peri-apse).

3 VIF_{ansa} is expressed in m, assuming 137.49 km/pixel in 2003; the uncertainties are the standard deviation between the individual VIFs.

4 Ratio in VIF_{ansa} between the years 2004 and 2003. We assumed 5% photometric calibration errors in addition to the quoted VIF errors.

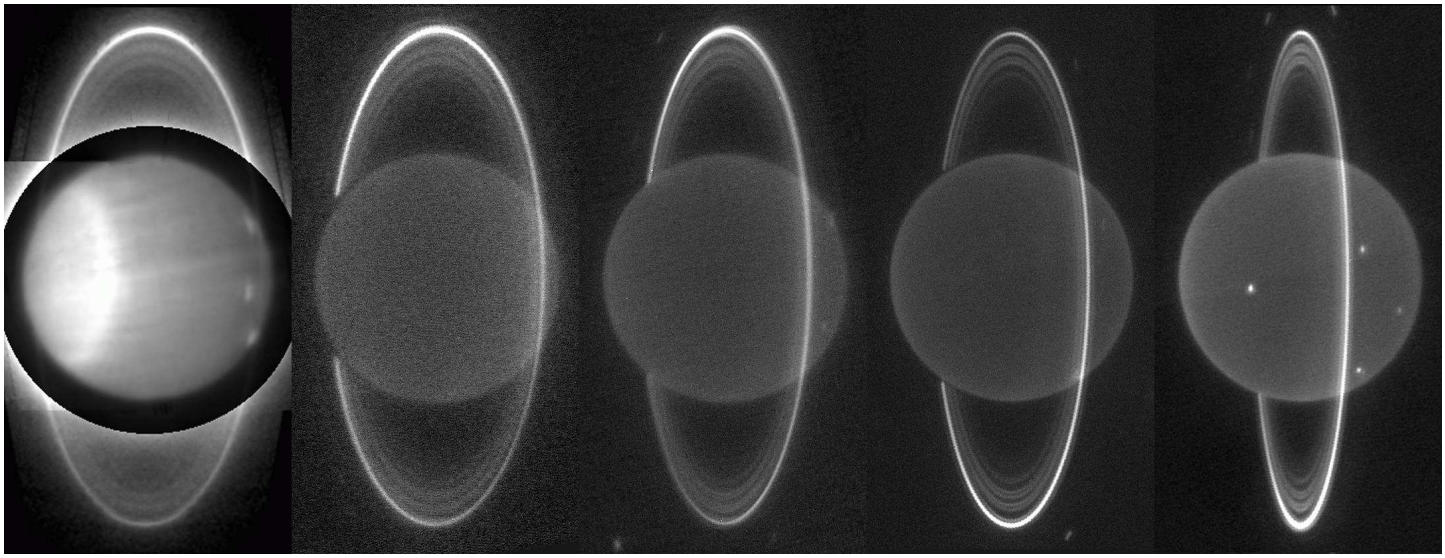

2000 2001 2002 2003 2004

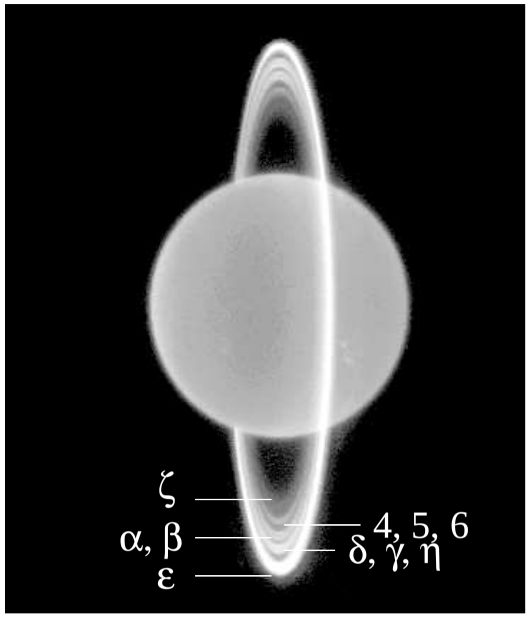

a

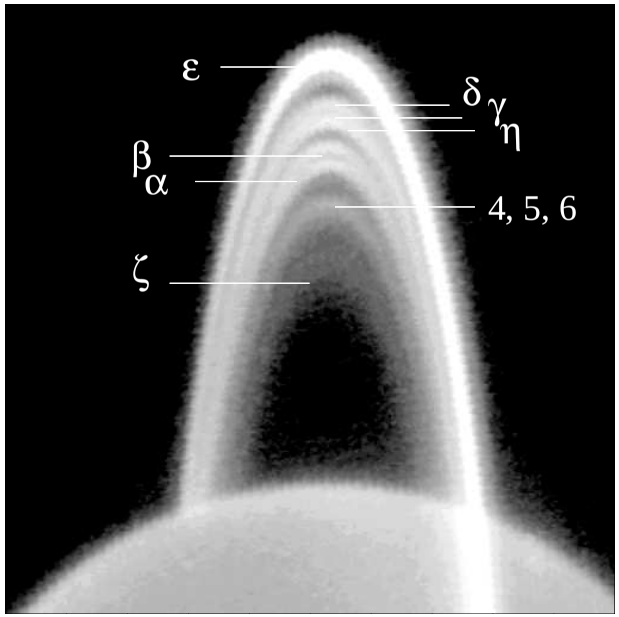

b

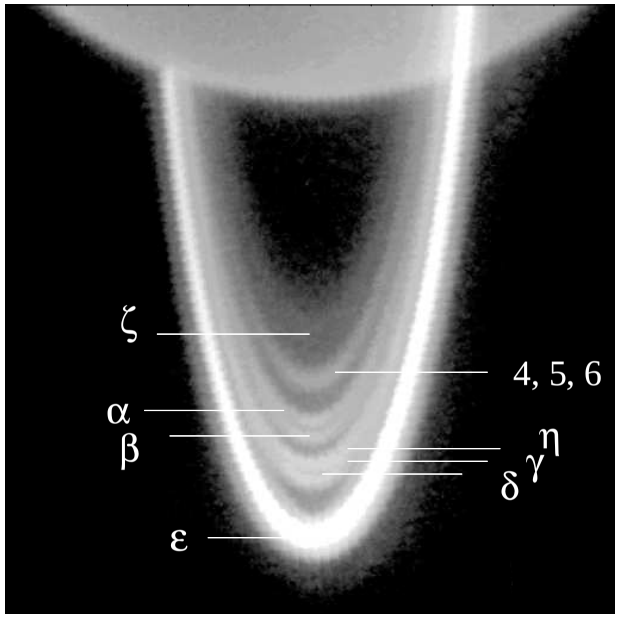

c

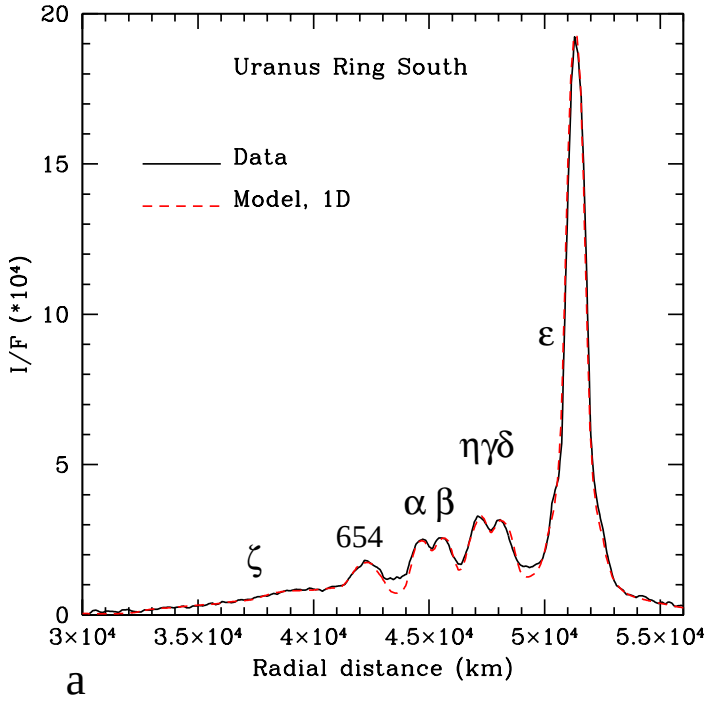
Uranus Ring South
Data
Model, 1D
I/F (*10⁴)
Radial distance (km)
ζ
654
α β
ηγδ
ε
a

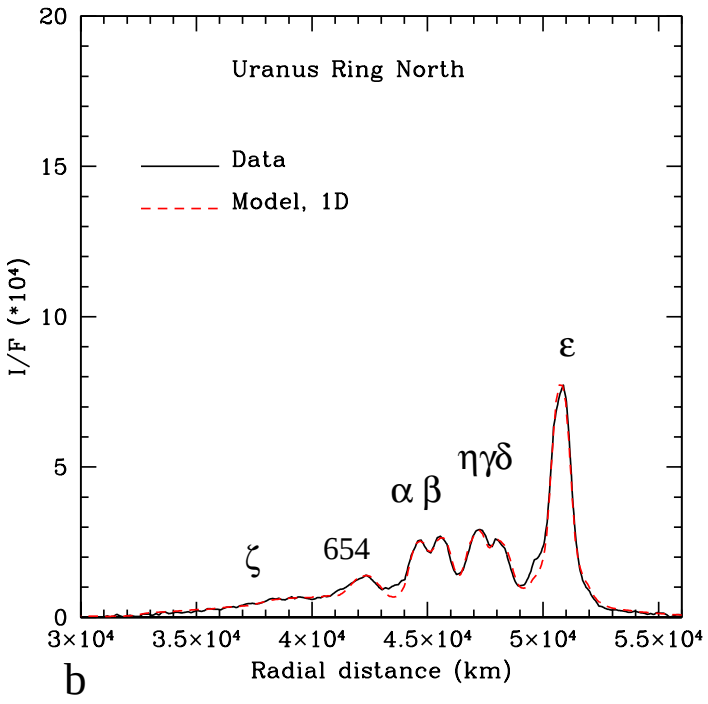
Uranus Ring North
Data
Model, 1D
I/F (*10⁴)
Radial distance (km)
ζ
654
α β
ηγδ
ε
b

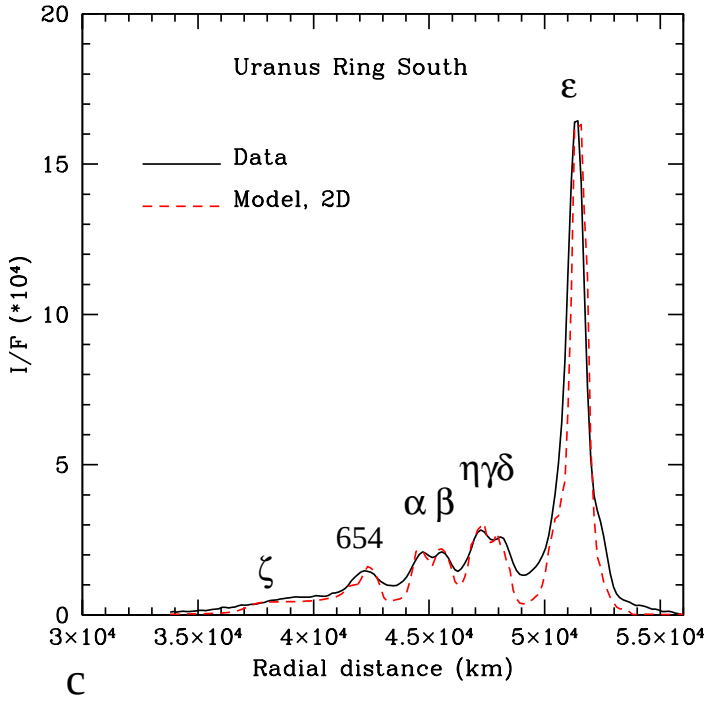
Uranus Ring South
Data
Model, 2D
I/F (*10⁴)
Radial distance (km)
ζ
654
α β
ηγδ
ε
c

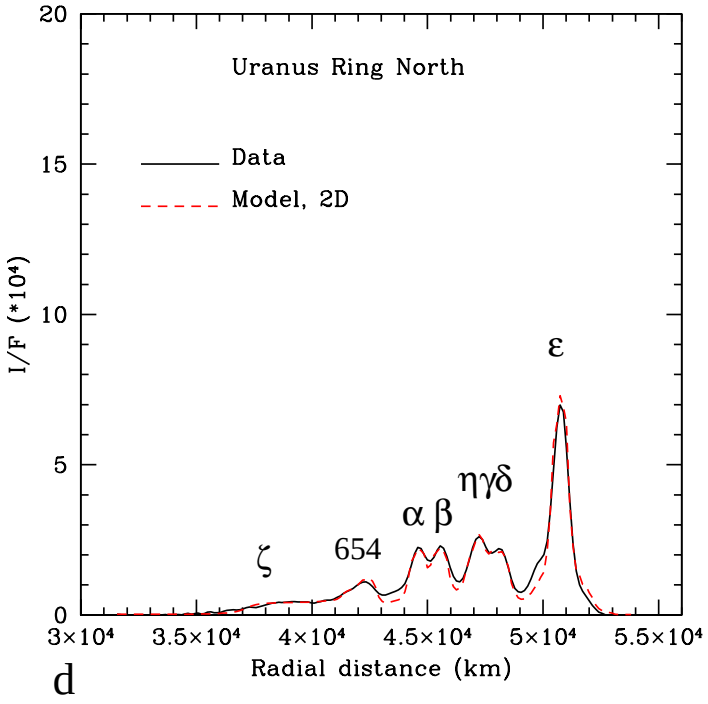
Uranus Ring North
Data
Model, 2D
I/F (*10⁴)
Radial distance (km)
ζ
654
α β
ηγδ
ε
d

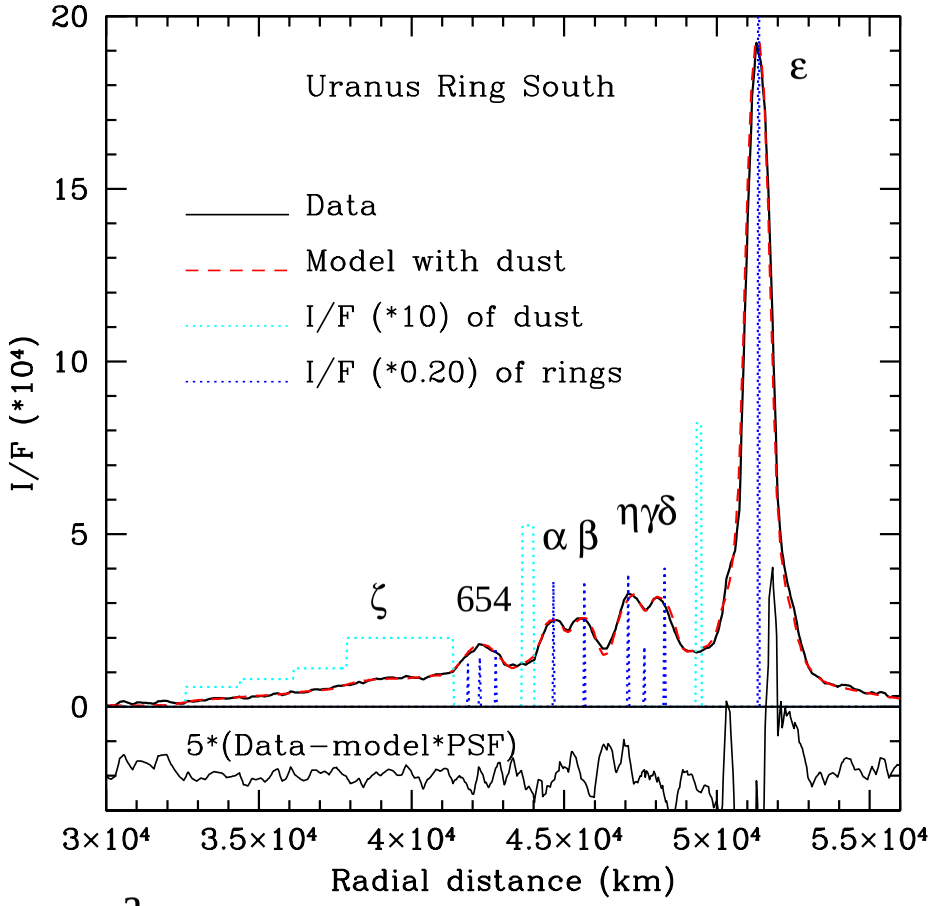
Uranus Ring South
Data
Model with dust
I/F (*10) of dust
I/F (*0.20) of rings
ε
α β
ηγδ
ζ
654
5*(Data−model*PSF)
I/F (*10⁴)
Radial distance (km)
20
15
10
5
0
3×10⁴
3.5×10⁴
4×10⁴
4.5×10⁴
5×10⁴
5.5×10⁴

a

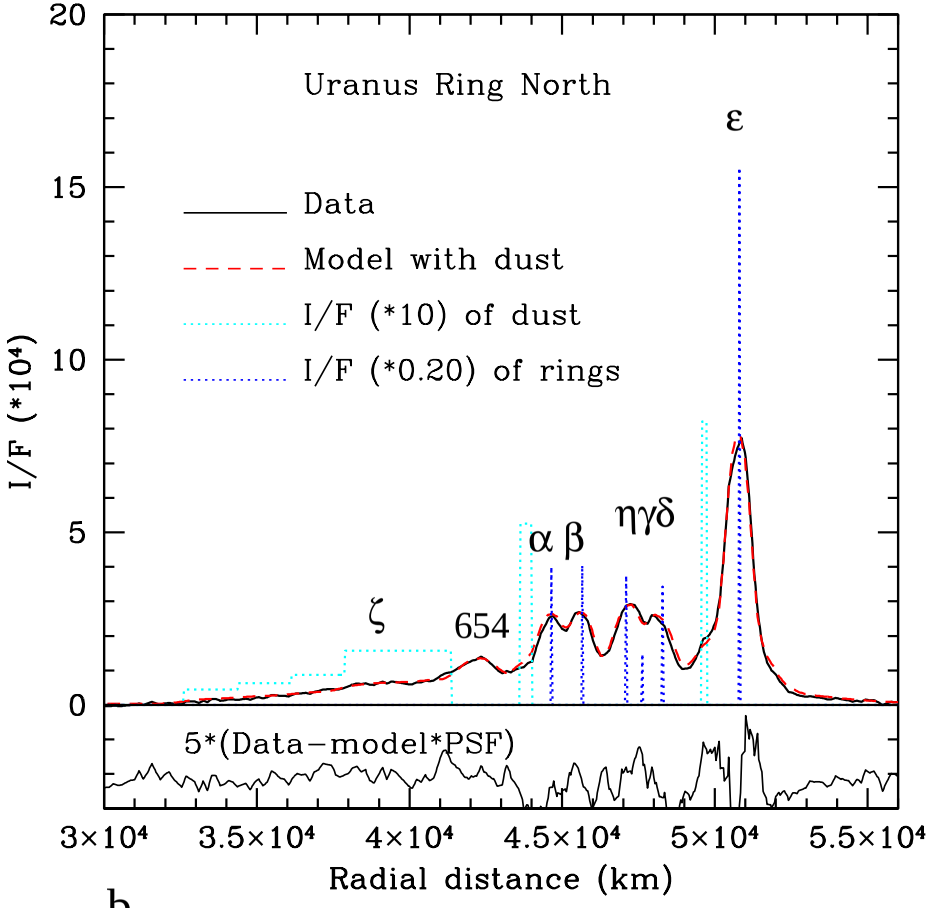
Uranus Ring North
Data
Model with dust
I/F (*10) of dust
I/F (*0.20) of rings
ε
α β
ηγδ
ζ
654
5*(Data−model*PSF)
I/F (*10⁴)
Radial distance (km)
20
15
10
5
0
3×10⁴
3.5×10⁴
4×10⁴
4.5×10⁴
5×10⁴
5.5×10⁴

b

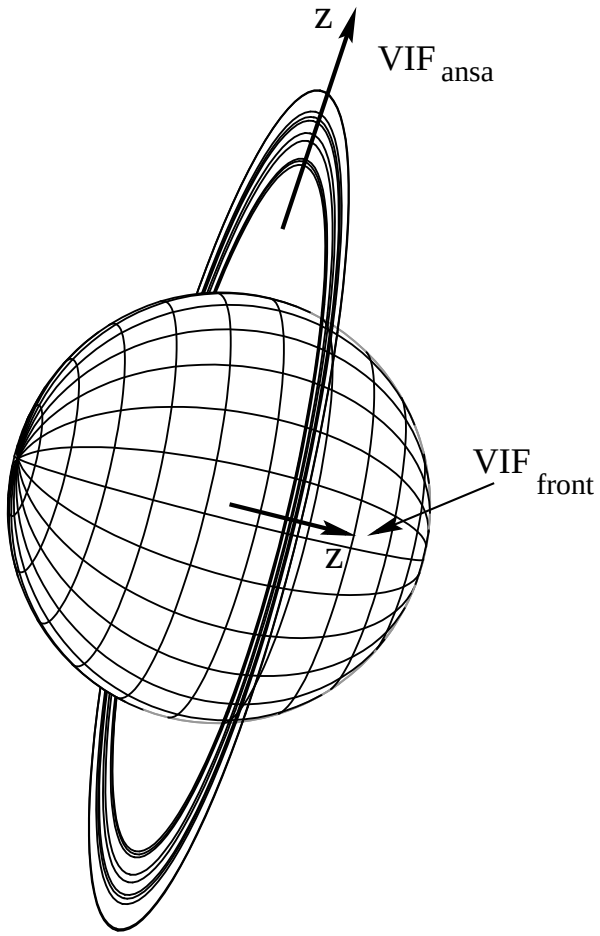
z
VIF ansa
VIF front
z